Accurate X-corner Fiducial Marker Localization in Image Guided Surgery (IGS)

Thomas Kerstein[1], Hubert Roth[2] and Jürgen Wahrburg[1]

[1]*Center for Sensor Systems (ZESS), University of Siegen, Paul-Bonatz-Straße 9-11, 57076 Siegen, Germany*
[2]*Institute of Control Engineering, University of Siegen, Hölderlinstr. 3, 57076 Siegen, Germany*

Keywords: X-corner, Fiducial Marker, Optical Localization, Image Guided Surgery (IGS), Corner Detection.

Abstract: In this paper a novel approach for reliable detection and accurate localization of X-corner fiducial markers is presented, which is particularly designed for Image Guided Surgery (IGS). The key idea is to combine two meaningful basic topological characteristics to one boosted filter providing adequate detection reliability and localization accuracy. Additionally and in contrast to conventional, retroreflective planar or spherical markers, X-corner fiducials facilitate not only position measurements with high precision but provide additional orientation information for improving distinction of multiple fiducials arranged within a geometrical reference structure. Experiments reveal robustness to considerable perspective distortion as well as invariance to illumination changes. Furthermore the presented approach offers high computational efficiency and a high level of flexibility for application-specific system design.

1 INTRODUCTION

Synthetic landmarks in form of X-corners (Figure 1, 2) provide high quality reference points for various visual localization tasks in photogrammetry and computer vision, most notably in context of camera calibration and crash tests in the automotive sector.

As a matter of principle, X-corner fiducials can be localized with high precision even if only a small area around the centre is visible. In contrast, accurate localization using planar or spherical markers requires the total marker area to be visible and free of contamination as the position is determined by computing the centre of this area. Further benefits are simple manufacturing by printing and mounting just by sticking.

In this paper we mainly focus on detection and localization of X-corner fiducials with regard to specific demands of Image Guided Surgery (IGS). Usually at least three markers are combined to form a discrete reference body (DRB) which is used to determine position and also orientation of an object, using Stereo Vision technique. Due to identical appearance of each marker, a common DRB can solely be identified by regarding the distances between all associated markers as the only relevant distinctive feature. Therefore a unique geometry constraint has

to be considered for DRB design. In this regard X-corners can help to reduce this limitation by providing an additional distinctive feature in terms of orientation of the edges between bright and dark sectors in conjunction with the arrangement of these sectors with respect to the centroid. Thus, X-corners strongly facilitate the design of customized DRBs.

The main contribution consists in the combination of two discriminative topological features to an efficient operator which offers reliable detection and accurate localization added by the reconstruction of the edge orientations. The method is proposed to be embedded into a proprietary optical 3D localization framework combined with a navigated surgical robot assistance system which along with the desired system modularity implies the following demands:

- Access to all relevant parameters allowing for a high level of flexibility instead of the black box character of a commercial digitizing system such as "MicronTracker®" by *Claron Technology Inc.* (Gibbons, 2011).
- Real time capability due to control oriented demands of a navigated robot system.
- Accuracy in the sub-millimetre range according to general requirements in IGS.
- Rapid design of customized DRBs allowing for reliable identification combined with less

restrictive design rules / limitations regarding the unique geometry constraint.

- General approach for facilitating the use of different stereo camera configurations.
- Robustness to significant perspective distortion and large variation of global and local illumination conditions, e.g. due to partial shading.
- Providing an extendable and universal experimental platform for evaluation.

2 RELATED WORK

2.1 Image Guided Surgery (IGS)

Optical 3D localization systems provide the foundation for applications in IGS to permanently acquire the spatial position of surgical instruments with regard to the patient's anatomy. In order to provide this functionality, both the patient and all surgical tools are typically equipped with fiducial based DRBs which are observed by a stereo camera as depicted in Figure 1 for an Image Guided Biopsy application.
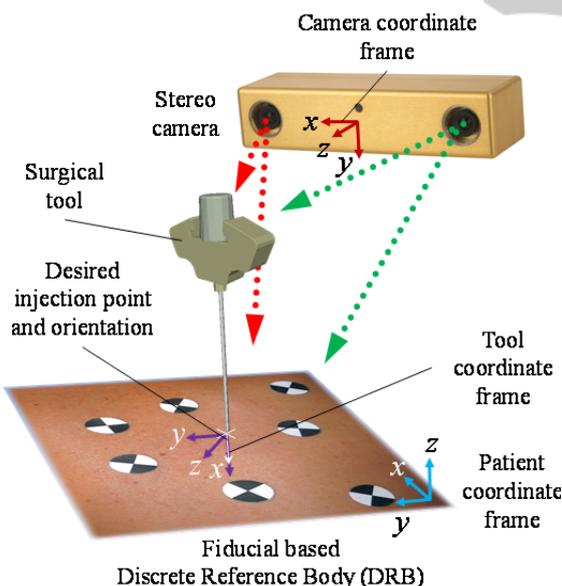

Figure 1: Typical setup of stereo vision-based 3D localization for surgical interventions shown for an Image Guided Biopsy scenario. Both patient and surgical tools (here the biopsy needle) are equipped with DRBs consisting of at least three fiducial markers which are detected and localized within both images of the stereo camera. By applying stereo triangulation, the objects' positions and orientations (represented by associated coordinate frames) are reconstructed. Thus, they can be spatially related to one another.

The processing pipeline for the optical 3D localization of a DRB basically consists of the following four steps:

1. Detection and 2D localization of single markers in both images of the stereo camera
2. 3D reconstruction of the 2D positions computed in step 1 applying stereo triangulation
3. Distance-based identification of the reference body geometry by assigning the markers to the DRB
4. Computation of position and orientation of the DRB using an appropriate registration method

This paper focuses exclusively on the 2D detection and localization of the fiducial markers in the first step, which has the most significant impact on the overall localization result. Conversely, all other steps which are provided by well-proven standard methods like stereo triangulation and registration immediately depend on the accurate 2D localization.

2.2 X-Corner Detection and Localization

Due to broad utilization of X-corners, especially for camera calibration using planar chessboards, a lot of research has been put into methods for detection and localization of which only a minor subset can be addressed here. Many approaches are particularly designed for camera calibration, which due to the regular structure of chessboards can benefit both from additional context information (equal corner distances) and consistent illumination conditions across the overall chessboard area. Unfortunately this does not apply to general fiducial localization.

First of all, there is a broad class of more or less classical methods intended for general rather than for particular X-shaped corner detection. These include, among others, the Moravec algorithm (Moravec, 1980), being one of the first approaches, the Förstner (Förstner, 1987) or the SUSAN corner detector (Smith, 1997) to name only a few of them. Probably one of the most commonly used method within this class is the Harris Corner Detector (Harris, 1988). This method establishes a corner response function where corners are located at local maxima. However, as these locations just like those obtained by other general corner detection methods in general do not agree with X-corner centroids, these methods are not very appropriate for X-corner localization.

An enhanced method accounting for distinctive X-corner characteristics, primarily symmetry constraints is presented by Zhang et al. (Zhang, 2009). They propose a "quarter operator" intended for camera calibration. Symmetry, variance and intensity

distribution regarding each pixel are incorporated as additional constraints. Even though the approach is similar to the one presented here, their variance operator does not apply a differential principle like the skew symmetric operator in our approach, which thus offers inherently larger robustness to varying illumination conditions and perspective distortion.

A common and obvious strategy for X-corner localization is provided by the following two-stage method: In the first stage corners are localized with pixel accuracy by a conventional corner detector like (Harris, 1988). In the second step localization is refined to subpixel accuracy by fitting a quadratic function to the interpolated intensity profile within close-up range around these preliminary corners and computing their extrema (Jain, 1995). However resulting from the first stage the close-up window might be decentred several pixels to the true centroid and least square fitting is generally sensitive to outliers. Thus surface fitting may lead to significant localization errors. For increasing accuracy and processing speed, Lucchese et al. (Lucchese, 2002) propose an alternative method without surface fitting by computing first and second order partial image derivatives on the local intensity profile and computing the extrema by morphological shrinking. However this method is not capable to capture the characteristic X-corner topology with the same quality as achieved by a particularly designed algorithm.

A more recent approach is proposed by Chen et al. (Chen, 2005), who apply a second order Taylor polynomial describing the local intensity profile around a preliminary corner. In (Zhao, 2011) an automated X-corner detection algorithm (AXDA) is presented where an X-corner is localized as the intersection of straight lines which have been fitted into the local intensity profile.

A further category of methods is formed by template-based approaches such as presented by (Arca, 2005) and (Xu, 2011) which is, just like ours, intended for surgical robot applications in the style of (Gibbons, 2011) rather than for camera calibration.

Finally, to provide a last method, recently a novel approach based on multiple weighted steerable matched filters (Mühlich, 2012) has been presented.

In conclusion, despite of the multitude of available approaches for X-corner detection and localization, each of those, listed here either exhibit a lack of robustness to variation of illumination conditions and perspective distortion and/or offers insufficient localization accuracy. All in all, this highly motivates the development of an X-corner detector which meets these crucial demands for IGS applications.

3 A NOVEL APPROACH FOR X-CORNER LOCALIZATION

Initially some important parameters of an X-corner fiducial marker should be defined.

- *Centroid* $\mathbf{c} = (c_x, c_y)$: point of intersection between the bright and dark areas.
- *Inward edges* $\{\mathbf{e}_{\mathbf{in},i}\}$ with $i \in \{1, 2\}$: edges between bright and dark sectors with a bright sector on its left and a dark sector on its right side, as seen from the centroid
- *Outward edges* $\{\mathbf{e}_{\mathbf{out},i}\}$ with $i \in \{1, 2\}$: complements of *inward edges*, with a dark sector on its left and a bright sector on its right side, as seen from the centroid.
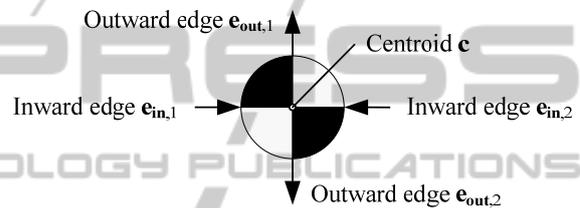

Figure 2: Topology of an X-corner fiducial marker, shown in the reference formation.

The processing pipeline of our approach comprises three main steps: (1) preselection of candidate fiducials, (2) accurate subpixel localization of the centroids and (3) determination of edge orientations as described explicitly in the following sections.

3.1 Preselection of Candidate Fiducials

As initial step Harris Corner Detection (Harris, 1988) is applied to the input image to identify corners approximately (usually within a range of few pixels around the true centroid). This step leads already to massive data reduction for further processing. Afterwards the number of wrong candidates is further reduced by applying intensity-based segmentation to a region of interest (ROI) centred on each corner. For a valid X-corner at least two distinct regions have to be identified. Finally the preliminary centroid is shifted and the ROI is re-centred to the balance point of the segmented regions.

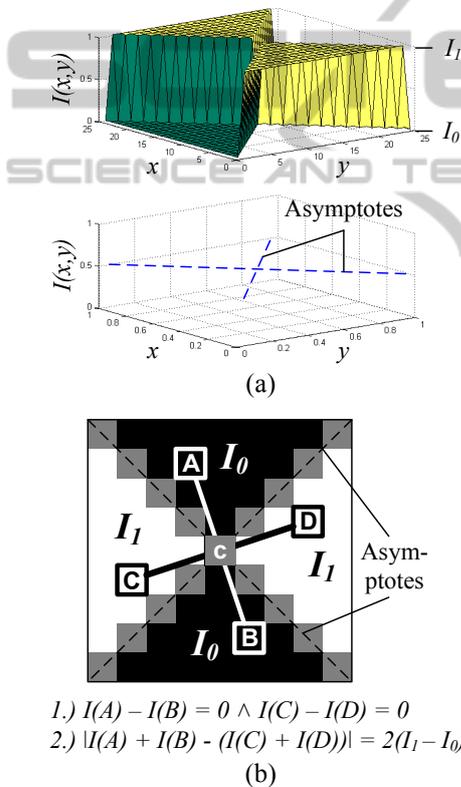## 3.2 Centroid Localization with Subpixel Accuracy

From a geometrical point of view, the shape of an X-corner can be approximated by a *hyperbolic paraboloid* with the *z*-axis parameterizing the pixel intensi-

ty $I(x, y)$. For an "ideal", unrotated X-corner the hyperbolic paraboloid takes a degenerated form as depicted in Fig. 3a. In this case any hyperbola in a section plane parallel to the x-y-plane consists only of their asymptotes being orthogonal to each other (degenerated equilateral hyperbola) and intersecting in the centroid of the X-corner given by the form:

$$y - c_y = \pm(x - c_x) \Longrightarrow y = c_y \pm (x - c_x). \quad (1)$$

Thus, given the centroid the two following characteristics (cf. Figure 3b) can be derived:

1. Two-fold rotational symmetry with respect to the centroid (central symmetry).
2. Axial skew-symmetry (anti-symmetry) with respect to the asymptotes of any sectional hyperbola parallel to the x-y-plane.

(a)

1.) $I(A) - I(B) = 0 \land I(C) - I(D) = 0$
2.) $|I(A) + I(B) - (I(C) + I(D))| = 2(I_1 - I_0)$

(b)

Figure 3: X-corner modelled as a hyperbolic paraboloid. (a) Degenerated form (top) and asymptotes of the sectional hyperbola in plane z = 0.5(bottom). (b) Illustration of mathematical constrains of X-corners with respect to individual pixels (A, ..., D) with a given intensity $I(x, y)$.

3.2.1 Combination of Discrete Symmetry Functions

For precise calculation of the centroid to pixel accuracy from a given input image two discrete functions, F_S (central symmetry) and F_A (skew-

symmetry) are derived from the developed constrains which both of them exhibit a differential computation scheme. After these functions have been applied to each pixel in the respective ROI, the centroid corresponds to the position of a global extremum related to each function respectively.

For increasing detection reliability and localization accuracy due to noise, the functions operate on groups of pixels rather than individual pixels as depicted in Figure 3b. Given a quadratic image region of $n \times n$ pixels ($n = 2k + 1, k \geq 1$) the discrete function operators $F_S \in \mathbb{Z}^{n \times n}$ and $F_A \in \mathbb{Z}^{n \times n}$ are formulated as follows:

- Central symmetry:

$$F_s(x, y) = \frac{1}{n^2} \sum_{\alpha, \beta = -k}^{k} |I(x + \alpha, y + \beta) \\ - I(x - \alpha, y - \beta)| \quad (2)$$

- Axial skew-symmetry:

$$F_A(x, y) = \frac{1}{n^2} \sum_{\alpha, \beta = -k}^{0} |I(x - \alpha, y - \beta) \\ + I(x + \alpha, y + \beta) \\ - I(x - \beta, y + \alpha) \\ - I(x + \beta, y - \alpha)| \quad (3)$$

Regarding F_S, the position of the centroid corresponds to the position of its global minimum $\min_{x,y} F_S(x, y)$ in the ROI, whereas considering F_A, it corresponds to the position of its global maximum $\max_{x,y} F_A(x, y)$.

Since it is inconvenient for computation to regard both functions separately, they are combined to the overall objective function $F_X \in \mathbb{Z}^{n \times n}$ in which the centroid is consistently identified at the position of the global maximum:

$$F_X = \begin{cases} 0, & \hat{F}_A < \hat{F}_S \\ \hat{F}_A - \hat{F}_S, & \hat{F}_A \geq \hat{F}_S \end{cases} \quad (4)$$

Here $\hat{F}_A$ and $\hat{F}_S$ are the normalized discrete functions with respect to their arithmetic averages $\overline{F_A}$ and $\overline{F_S}$ respectively:

$$\hat{F}_S(x, y) = \frac{1}{\overline{F_S}} F_S(x, y) \quad (5)$$

$$\hat{F}_A(x, y) = \frac{1}{\overline{F_A}} F_A(x, y) \quad (6)$$

Since the centroid of a valid X-corner always corresponds to a distinctive peak far above the average $\overline{F_X}$ (in general: $\max_{x,y} F_X \geq 3\overline{F_X}$), the maximum output of F_X is further utilized for indicating and rejecting wrong corner candidates. If it is beyond a given threshold $T; 1 \leq T \leq 3\overline{F_X}$ the centroid

$\mathbf{c} = (c_x, c_y)$ is computed with subpixel accuracy as the weighted average of F_X across the region:

$$\mathbf{c} = (c_x, c_y)$$
$$= \left(\frac{\sum_{i=1}^{n} F_X(x_i, y_i)\, x_i}{\sum_{i=1}^{n} F_X(x_i, y_i)}, \frac{\sum_{i=1}^{n} F_X(x_i, y_i)\, y_i}{\sum_{i=1}^{n} F_X(x_i, y_i)} \right) \qquad (7)$$

3.2.2 Function Representation in Form of Template Masks

F_S and F_A can be conveniently represented in form of template masks being applied to an input image. These masks virtually consist of "positive" and "negative" areas. Concerning F_S one pair of opposite pixels is involved in each step of calculation whereas concerning F_A two pairs of opposite pixels are involved. The result of each calculation step is the

difference between respective pixel values in "positive" and "negative" regions.

Both masks and the effect of applying these masks to an example input image of an X-corner fiducial are depicted in Figure 4.

3.3 Determination of Edge Orientation

Due to the two-fold rotational symmetry with respect to its centroid, the edge orientations of an X-corner are unique only up to a rotation of 180 degrees. Thus, edge orientation does not provide a unique measure but largely helps as an additional distinctive feature to reduce the risk of misidentification of a particular reference body configuration which is used during a surgical intervention.
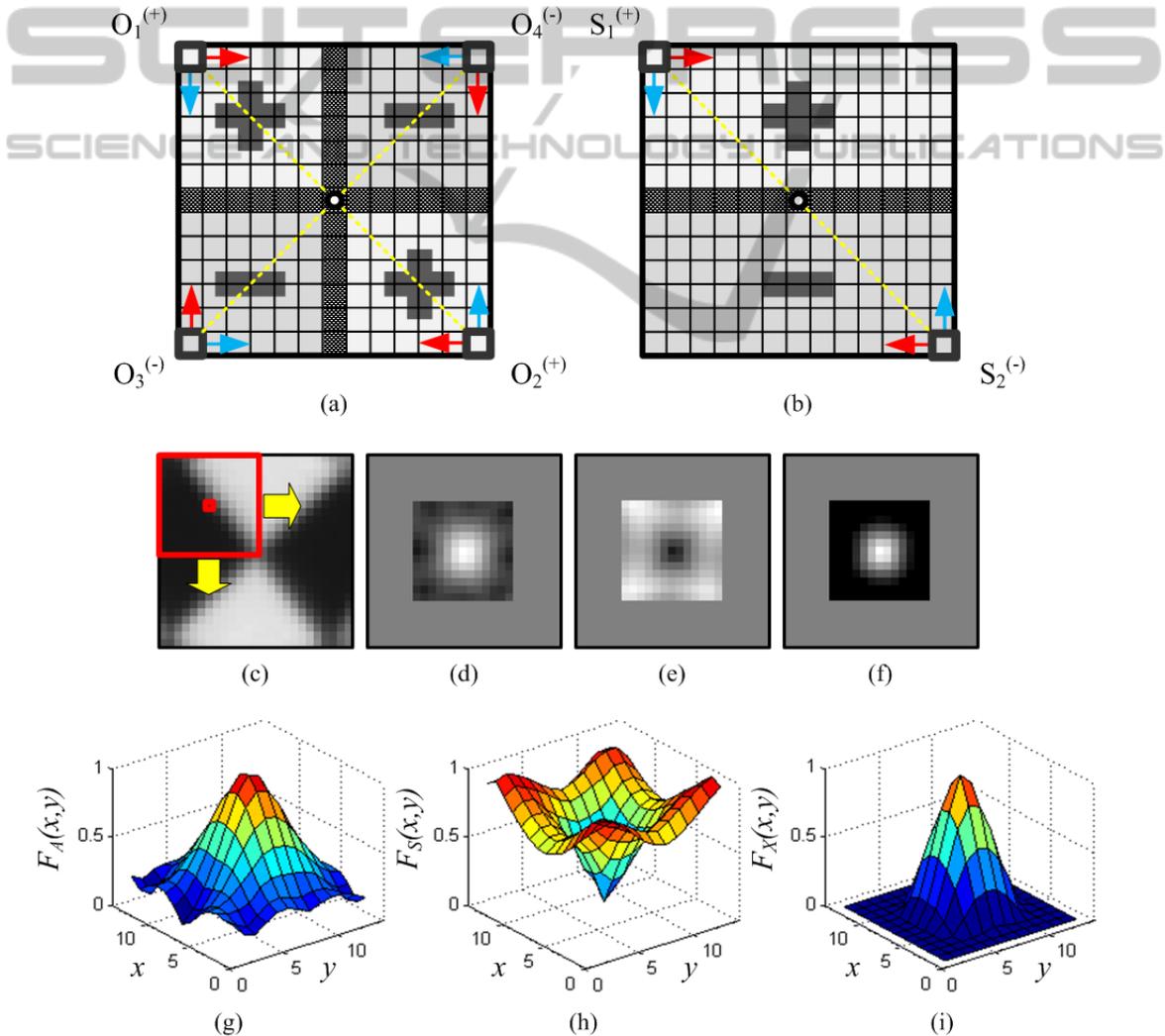

Figure 4: Template masks for X-corner fiducial localization and results. (a) Template mask for F_A. (b) Template mask for F_S. (c) Applying a mask to an input image. (d) Output of F_A. (e) Output of F_S. (f) Final output of F_X. (g) – (i) 3D-surface representation of function outputs of F_A, F_S and F_X normalized to [0,1].

The edge orientations are determined by computing the orientation of the main axes of a *hyperbolic paraboloid* fitted to the smoothed close-up view around the centroid (Figure 5a) by solving the following objective function (Equation 8) in least squares sense (Jain, 1995):

$$\min_{A,...,F} \|Ax^2 + Bxy + Cy^2 + Dx + Ey + F \\ - I(x,y)\|^2 \quad (8)$$

Here $\{A, ..., C\}$ are the (unknown) coefficients of the implicit form of a hyperbolic paraboloid and $I(x,y)$ is the pixel intensity at a given position $\mathbf{x} = (x,y)$ (Figure 5b).

In order to account for hyperbolic paraboloids rather than for elliptical paraboloids, the discriminant Δ must be constrained to $\Delta = AC - B^2 < 0$. However, since we already know the shape, the discriminant can be ignored.

Afterwards the rotation angle ϕ between the *transverse* axis (*semi-major* axis) and the x-axis can be computed:

$$\tan 2\phi = \frac{2B}{A - C} \quad (9)$$

Since it is not specified if the *transverse* axis coincides with the bright or the dark sectors, the comparison of A and C must be analyzed as an additional criterion. Finally the rotation angle $\acute{\phi}$ of the fiducial relative to its reference orientation can be computed and thus the edge correspondences for $\{e_{in,i}\}$ and $\{e_{out,i}\}$ can be derived (c.f. Figure 5c):

$$\acute{\phi} = \begin{cases} \phi + \dfrac{\pi}{4}, A > C \\ \phi - \dfrac{\pi}{4}, A \le C \end{cases} \quad (10)$$
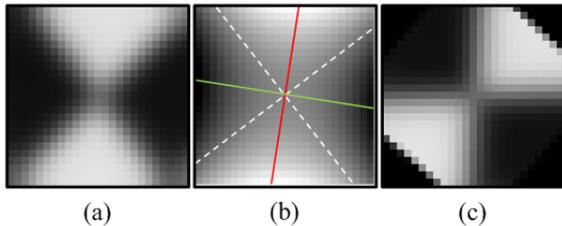
Figure 5: Determining edge orientations of an X-corner fiducial: (a) Input image (ROI) after Gaussian smoothing. (b) Resulting hyperbolic paraboloid obtained by linear least squares fitting (asymptotes: white dashed lines, semi-major axis: red solid line, semi-minor axis: green solid line). (c) Fiducial rotated by $\acute{\phi}$ to its reference orientation.

4 EXPERIMENTAL RESULTS

In this section, the performance of the proposed approach is evaluated in terms of processing speed, localization accuracy with respect to different distances and viewing angles and robustness as significant criterions for IGS. The experiments were performed on an Intel Core™2 Quad @2.5GHz CPU using a stereo camera of type *PointGrey Bumblebee BB2-03S2M-60* (Point Grey, 2013) with a baseline of 120 mm, a focal length of 6 mm, a field of view of 43 degrees and a resolution of 640×480 pixels.

4.1 Processing Speed

In the first experiment the runtime performance is analyzed. For this purpose 1000 samples are recorded and the average time consumption is evaluated.

The by far most significant portion of processing time is required by Harris Corner Detection in the preselection step, explicitly over 10 ms for the given image resolution. However to our experience it is sufficient to execute corner detection on a downscaled version of the input image of half width and height respectively. Thus, time consumption of this step can be reduced by a factor of 4 to 2.52 ms. All other steps amount only 13% in total of the overall processing time, explicitly 0.16 ms for centroid computation and 0.21 ms for orientation computation, summing up to an average time consumption of 2.89 ms in total for the complete detection and localization of an X-corner fiducial marker.

4.2 Localization Accuracy

In the next experiment, the effect of varying marker positions and orientations on the 2D as well as the 3D localization accuracy is evaluated.

4.2.1 2D-Localization Accuracy

First of all the 2D localization error, defined as the *Euclidian* distance between the measured and the target position of a fiducial is utilized and regarded as a function of its position and orientation.

Since it is hardly possible to acquire the ground-truth 2D marker-position with respect to the image coordinate system of the camera using real image data, the localization accuracy is examined by simulation. For this purpose, a single camera module of the stereo camera is modelled by using *OpenGL* according to the actual camera parameters.

A square X-corner fiducial with a side length of 24 mm is placed within the virtual scene wherein the pose is provided externally by the system. The reference pose is chosen on the optical axis at a distance of 500 mm in front of the camera and without any rotation. To allow for a reproduction as realistic as

possible, both additive and multiplicative pixel noise (amplifier and shot noise) is added to the scene.

In order to provide a reference to state-of-the-art X-corner localization, the measurements are also performed with the "quarter operator" (QO) presented in (Zhang, 2009) (c.f. 2.2) which follows a similar approach as the one presented in this paper.

All parameters are varied individually in order to expose distinctive characteristics and progressions. Position components are varied within steps of 1 mm, while rotation angles are varied within steps of one degree. The results are shown in Figure 6. Here always a number of samples (50 for z and 10 for all other dimensions) are averaged together to achieve a better illustration.

Referring to these measurements, the localization error is always much less than one pixel. Regarding x, y and ψ, the marker is detected in the whole range with a mean localization error of even less than 0.04 pixels. Regarding the distance z between camera and marker, reliable detection is provided up to at least 1800 mm. The detection range is primarily limited by the focus range of the camera and the projected size of the marker on the imager, which must not be less than 9×9 pixels. The smaller the mask, the larger is the maximum measurement distance but the smaller is the available resolution. For the given configuration the optimal scale of the fiducial relative to the imager of the camera is at about 500 mm.

Regarding pan ϕ and tilt θ, reliable detection is provided up to at least 50 degrees. Here the localization error does not exceed 0.1 pixels in this range, whereas beyond, measurement uncertainties due to perspective distortion become noticeable.

Our approach outperforms the quarter operator in almost the entire measuring range, especially in presence of large perspective distortion (ϕ, θ) where localization most notably benefits from the differential principle of the skew symmetric operator.

4.2.2 3D-Localization Accuracy

For providing a more practice-oriented accuracy measure for IGS, additionally the 3D localization error is evaluated using the real stereo camera. In contrast to the 2D localization error, this is achieved as the mean deviation between known and measured distances of 25 markers distributed on a grid (with well known distances) to the particular one which is placed at the position in question. The distance to the camera is varied from 200 to 1200 mm. For determining orientation the grid is accordingly rotated.

Here the distance deviation is always less than 0.5 mm. Regarding x, y and ψ, it is even less than
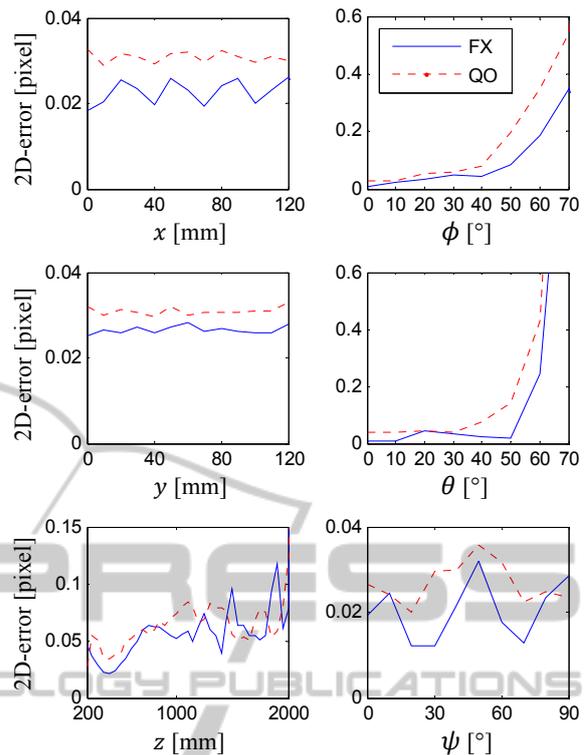

Figure 6: Comparison of the 2D localization error of an X-corner fiducial subject to its position (left) and orientation (right), between the computation with the proposed approach (FX; solid line) using F_X and the "quarter operator" (QO; dashed line) presented in (Zhang, 2009).

0.1 mm within the whole range, whereas at a distance of $z = 1000$ mm, it has been measured with 0.45 mm. Regarding ϕ and θ the distance deviation is below 0.25 mm in the range of 0 to 50 degrees.

4.3 Robustness

Finally robustness of detection and localization is analysed by positioning fiducials within a wide distance and orientation range combined with strongly varying illumination conditions. 32 successful results for poor image quality are shown in Figure 7.

5 CONCLUSIONS

We have presented a novel technique for reliable detection and accurate localization of X-corner fiducial markers with regard to specific demands of IGS providing the perspective to be combined with a navigated surgical robot assistance system. For detection and localization fundamental topological features are combined to an efficient detector.
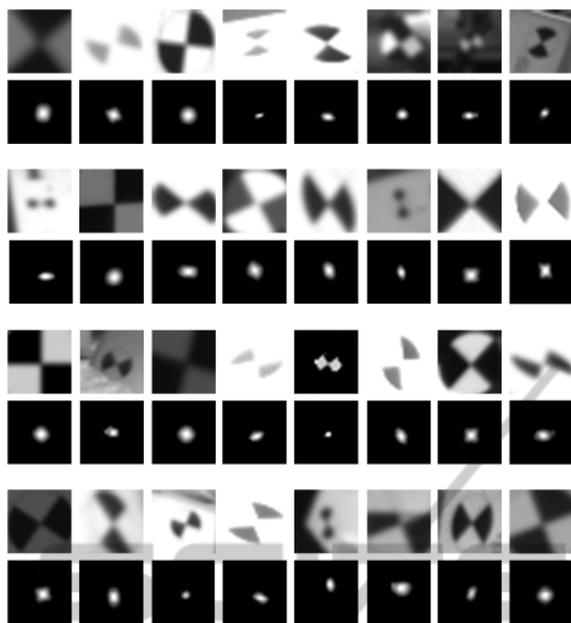
477

Figure 7: Selection of 32 different samples of X-corner fiducials from real-world scenes and corresponding processing results (ROI size: 27×27 pixels). Upper rows: Sample images (Input images). Lower rows: Results of applying F_X to the input images. Note the large variations regarding both illumination and perspective distortion.

Major advantages include highly flexible system design possibilities in conjunction with real time capability and localization accuracy in the subpixel / sub-millimetre range. Further benefits are robustness to large variation of both illumination conditions and perspective distortion. The additional determination of the edge orientations of an X-corner provides an additional distinctive feature for improving detection reliability of a certain reference body template and therefore attenuates the restrictive unique geometry constraint of reference bodies consisting of conventional fiducial markers used for IGS. For that reason and due to simple mounting of X-corner fiducials just by sticking on an object, the presented approach is predestined for rapid and flexible DRB design.

In future research the corresponding advantages for simpler patient tracking will be investigated.

REFERENCES

Arca, S., Casiraghi E., Lombardi, G., 2005. Corner Localization in chessboards for camera calibration. *IADAT-micv2005*, Madrid.

Chen, D., Zhang, G., 2005. A New Sub-Pixel Detector for X-Corners in Camera Calibration Targets. In *Proceedings of WSCG (Short Papers)*, pp. 97-100.

Förstner, W., Gülch, E., 1987. A Fast Operator for Detection and Precise Location of Distinct Points, Corners and Centres of Circular Features. In *ISPRS Intercommission Workshop, Interlaken*, pp. 149-155.

Gibbons, M., 2011. In Need of a Keen Eye - Stereo Vision-Based Optical Tracking Yields New Surgical Tools. *Inspect-online - Imaging and Machine Vision*, http://www.inspectonline.com. Vancouver.

Harris, C., Stephens, M., 1988. A combined corner and edge detector. In *Proceedings of the Fourth Alvey Vision Conference*. Manchester, pp. 147-151.

Jain, R., Kasturi, R., Schunck, B.G., 1995. *Machine Vision, McGraw-Hill, Inc.*, New York, NY.

Lucchese, L., Mitra, S. K., 2002. Using Saddle Points for Subpixel Feature Detection in Camera Calibration Targets. In *Proceedings of the 2002 Asia Pacific Conference on Circuits and Systems, Singapore*, pp. 191-195.

Moravec, H., 1980. Obstacle Avoidance and Navigation in the Real World by a Seeing Robot Rover. *Tech. Report CMU-RI-TR-3, Carnegie-Mellon University, Robotics Institute*.

Mühlich, M., Friedrich, D., Aach, T., 2012. Design and Implementation of Multi-Steerable Matched Filters. *IEEE Transactions on Pattern Analysis and Machine Intelligence (PAMI), Vol. 34, Issue 2*, pp. 279-291.

Point Grey Research, 2013. *Stereo vision Bumblebee2 web page:* http://www.ptgrey.com/products/bumblebee2, last visited on 2013-09-20.

Smith, S. M., Brady, J. M., 1997. SUSAN – a new approach to low level image processing. *International Journal of Computer Vision*, Vol. 23, No. 1, pp. 45–78.

Xu H., Sun, B., 2011. X-corner detection based on Segment Test Applied in optical pose tracking system. *International Symposium on Bioelectronics and Bioinformatics (ISBB)*, Suzhou, pp. 162-165.

Zhang, S., Guo, C., 2009. A Novel Algorithm for Detecting both the Internal and External Corners of Checkerboard Image. *ETCS '09, First International Workshop on Education Technology and Computer Science*, Wuhan, pp. 975-979.

Zhao, F., Wei, C., Wang, J., Tang, J., 2011. An Automated X-corner Detection Algorithm (AXDA). In *Journal of Software*, Vol. 6, No. 5, pp. 791-797.